Appl. Phys. A (2015) 119:571–579
DOI 10.1007/s00339-015-8992-8

Applied Physics A
Materials Science & Processing

Study of carrier mobility of tubular and planar graphdiyne

Seifollah Jalili · Fatemeh Houshmand · Jeremy Schofield

Received: 16 August 2014 / Accepted: 9 January 2015 / Published online: 22 January 2015

Abstract Graphdiyne nanotubes were constructed 10 years after their theoretical prediction and many properties of them have remained unknown until now. In this investigation, transport properties of new family of carbon nanotubes, graphdiyne nanotubes, were studied systematically by using spin-polarized density functional theory coupled with Boltzmann transport equation with relaxation time approximation. We have predicted the charge mobility for tubular forms of graphdiyne (GDNT). The calculated intrinsic electron mobility for GDNT at room temperature can reach the order of 10^4 cm^2 V^{-1} s^{-1}. On the other hand, the hole mobility magnitude is about an order of 10^2 cm^2 V^{-1} s^{-1}. The DFT results also show that GDNT is direct band-gap semiconductor. The calculated cohesive and strain energies for GDNT indicate that this new nanomaterial is more stable than the conventional carbon nanotubes. Adsorption of a transition metal atom (Fe) on the external surface of GDNT has been studied by DFT method as well as density functional theory plus effective on-site Coulomb repulsion parameters U, Hubbard correction. Transition metal (TM)-adsorbed GDNT is magnetic and shows semimetal property. Charge transfer between TM adatom and GDNT as well as the electron redistribution of the TM intra-atomic s, p and d orbitals indicates that the TM-adsorbed single-walled γ-graphdiyne have a high potential for applications in spintronics and in future optoelectronics. The single-layer nanostructure of graphdiyne (pGD) is studied too. The resulted electronic properties of pGD and TM-absorbed-pGD confirm previous results for these nanostructures. Also, transport properties of stable TM-pGD nanostructure as well as TM-GDNT are notable. Energy gap values for both nanostructures are found to be strongly sensitive to the local Coulomb interactions U of the TM d orbitals.

S. Jalili (✉) · F. Houshmand
Department of Chemistry, K. N. Toosi University of Technology, P. O. Box 15875-4416, Tehran, Iran
e-mail: sjalili@kntu.ac.ir

S. Jalili
Computational Physical Sciences Research Laboratory, School of Nano-Science, Institute for Research in Fundamental Sciences (IPM), P.O. Box 19395-5531, Tehran, Iran

J. Schofield
Chemical Physics Theory Group, Department of Chemistry, University of Toronto, 80 Saint George Street, Toronto, ON M5S 3H6, Canada

1 Introduction

During recent years, the synthesis of a new allotrope of carbon, graphyne, or so-called s*upergraphene*, was reported [1]. This category of carbon-based materials has both sp^2 and sp-hybridized carbon atoms. These materials are predicted to have excellent electrical properties and chemical stability [2] and high conductivity [3], with a wide range of promising potential applications in electrical devices. In addition, it has been suggested that graphdiynes, other members of the graphyne family, which have two acetylenic linkages between their nearest-neighbor hexagonal rings, might be successfully utilized for gas purification and are mechanically stable for gas separation without a need for any chemical functionalization [4]. The graphdiyne (GD) structure was historically designed by Haley et al. [5]. So far, many unique features of graphdiyne such as its high-temperature stability and the semiconductive property with conductivity comparable to that of silicon [6] have been reported. Very recently, the preparation of GD nanowires with high conductivity and

mobility [3] and attempts to utilize the planar GD (pGD) as a component of polymer solar cells [7] were reported. Besides, the search for now, unknown till now, 0D–3D forms of graphdiyne such as onions, nanotoroids and nanotubes seems very desirable. This will lead to the expansion of the family of the discussed graphdiyne materials and to the discovery of their new 0D–3D forms with unexpected properties [8]. The construction of nanotubes of graphdiyne was reported few years ago [9]. However, to our knowledge, as yet, theoretical studies on the graphdiyne nanotube motifs have not been reported. The graphdiyne nanoribbon has been demonstrated to possess charge mobility as high as 2×10^5 cm^2 V^{-1} s^{-1} at room temperature [10]. It is the primary motivation of this work to predict the electronic properties and the intrinsic carrier mobility for graphdiyne single layer as well as nanotubes.

As there are many different types of graphdiyne structures, various new families of pure nanotubes can be generated from graphdiyne sheets that have different electronic and structural characteristics. Similar to carbon nanotubes (CNTs), which are formed by rolling up a graphene sheet, armchair, zigzag or chiral graphdiyne nanotubes (GDNTs) are possible. In this research, a (3, 3) nanotube of γ-graphdiyne has been studied. This is because γ-graphdiyne is known to have high-temperature stability and shows mechanical properties similar to graphene [10]. Manipulating the magnetic properties of planar sheets and nanotubes through transition metal (TM) adsorption is an important challenge for realizing their application in spintronics and nanoelectronics [11]. So we have also studied the effect of Fe transition metal adsorption on the selected systems.

2 Computational details

Density functional theory (DFT) calculations were performed using plane waves and ultra-soft pseudopotentials [12], implemented in Quantum Espresso package [13]. The electron exchange and correlation effects were considered through the generalized gradient approximation (GGA) with Perdew–Burke–Enzerhof (PBE) approach [14], which is suitable for energy calculations and for estimating Kohn–Sham band gaps. The energy cutoff for the plane wave basis set was set to 500 eV.

Two-dimensional structure of single-layer graphdiyne (pGD) is shown in Fig. 1a. It is defined by two lattice vectors $\mathbf{a}_1 = a\mathbf{x}$ and $\mathbf{a}_2 = a/2(-\mathbf{x} + 3^{1/2}\mathbf{y})$, with $a = 9.45$ Å [15]. The rhombic unit cell of graphdiyne is drawn with a broken line in Fig. 1a. The unit cell internal coordinates (bond length and angles) were set according to Narita et al. [16] optimized structures.

A GDNT can be defined by the chiral vector $\mathbf{C}_h = n\mathbf{a}_1 - m\mathbf{a}_2$. According to this definition for the chiral vector, zigzag nanotubes are represented by (n, n) and armchair ones by (n, 0), which is opposite to carbon nanotubes. Here, we have studied a (3, 3) zigzag GDNT, Fig. 1b, which has 108 carbon atoms. A 108-carbon supercell was also used for pGD calculations, which is shown in Fig. 2 with a rectangle.

The pGD and GDNT systems were placed in orthorhombic and tetragonal boxes, respectively, with the dimensions given in Table 1. The optimized vacuum spaces in the z-direction for pGD (15 Å) and x- and y-directions for GDNT (15 Å) were included to avoid interactions along the non-periodic dimensions. The positions of atoms were fully optimized to get the equilibrium structures, using a convergence threshold of 0.01 eV/Å in force. The k-point sampling of the Brillouin zone was performed according to the Monkhorst–Pack scheme [17] using a $81 \times 81 \times 1$ grid for pGD and a $1 \times 1 \times 111$ grid for GDNT optimizations.

The mobilities of charge carries (hole and electrons) along two directions were evaluated by Boltzmann transport approximation with an in-house MATLAB (Matlab 2012) code [18].

3 Results and discussion

3.1 Energetic and structural properties

To evaluate the stability of the systems, cohesive energy was calculated from $E_{coh} = E_{tot} - nE_C$, where E_{tot} denotes the spin-polarized total energy of fully optimized planar or tubular graphdiyne. n and E_C are the number of carbon atoms and the total energy of a single carbon atom, respectively. Both energy terms were evaluated using a same supercell size. Table 1 shows the results for pGD and GDNT. The calculated cohesive energy for p-GD is in agreement with the work of Narita et al. [16]. The cohesive energy for GDNT is higher than that of a carbon nanotube with similar radius [19], because of strong C≡C bonds.

Table 1 also shows the optimized carbon–carbon bond lengths for pGD and GDNT. The average length of single bonds between two triple bonds in both systems is lower than the value of 1.38 Å for diacetylene [16]. Compared with a carbon nanotube with the same radius, the bond length difference between planar and tubular forms is larger for the GDNT. The strain energy (the difference of cohesive energies between the sheet and tube) for GDNT (0.23 eV/atom) indicates that this tubular structure is more stable than the carbon nanotube with a same radius [20]. This high stability may be originated from inter-atomic moving electrons and effect of conjugated multiple bonds.

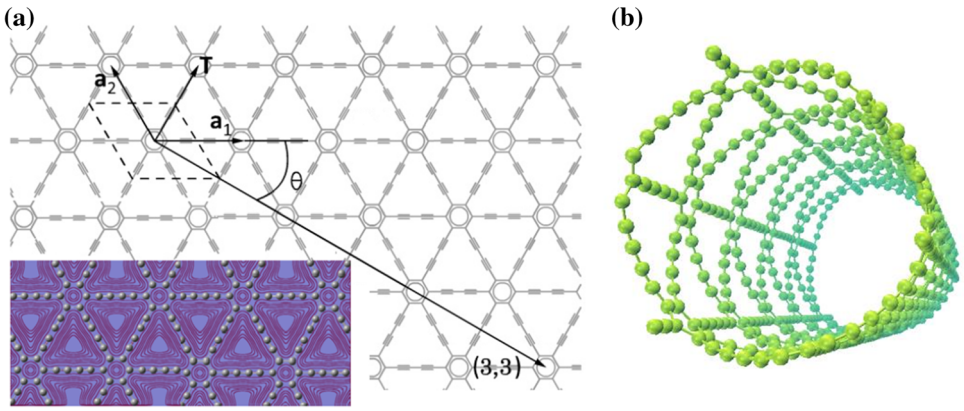

Fig. 1 **a** Chiral and transition vectors for a (3, 3) graphdiyne nanotube. Counter plot of charge density is shown at the *bottom*. The rhombus drawn with *dashed lines* represents the primitive cell. **b** Structure of the zigzag (3, 3) graphdiyne nanotube

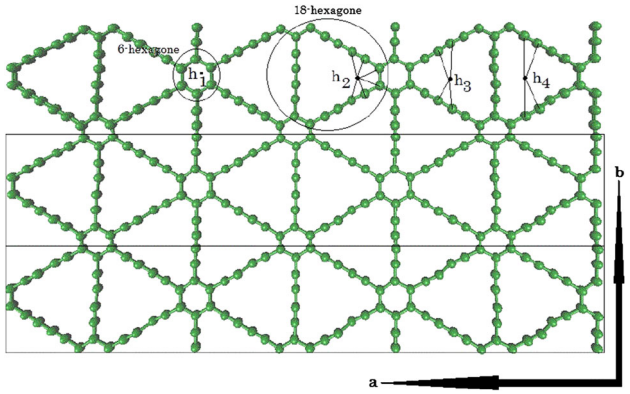

Fig. 2 Supercell used for pGD calculations, with 108 carbon atoms. The possible sites for adsorption of Fe on planar graphdiyne are also shown

Table 1 Structural parameters for pGD and GDNT systems

System	$a_{sc} \times b_{sc} \times c_{sc}$ (Å^3)	C(sp)≡ C(sp)	C(sp^2)– C(sp^2)	≡C– C≡	E_{coh} (eV/atom)
pGD	57.18 × 9.01 × 1.61	1.23	1.40	1.33	7.78
GDNT	18.10 × 18.10 × 9.01	1.24	1.39	1.30	8.01

The bond lengths are in Å

Consequently, the higher stability of GDNT can make this structure more interesting for new applications.

In order to study the effect of adsorption of a TM atom on the surface of pGD/GDNT, various adsorption sites for a single Fe atom were examined. Figure 2 shows these sites. The most stable position for adsorption of Fe atom for both structures is the **h2** site above a 18-hexagon. In this site, Fe forms six bonds with neighboring carbon atoms. Adsorption energies of Fe on pGD/GDNT are reported in Table 2. They were calculated from $E_{ads} = E_{TM+GD} - E_{GD} - E_{TM}$, where three energy terms are the spin-polarized total energies of TM-adsorbed pGD/GDNT, pure pGD/GDNT and an isolated TM atom, respectively.

Table 2 Structural parameters for Fe-adsorbed pGD and GDNT systems

System	d_{Fe-C} (Å)	h (Å)	E_{ads} (eV)	E^U_{ads} (eV)
Fe@pGD	1.83 (1.54)	0.99 (0.136)	−2.81	−3.07
Fe@GDNT	1.98 (1.75)	1.03 (0.480)	−4.93	−5.05

The numbers in parentheses are obtained from DFT + U calculations

Adsorption of Fe on both structures is exothermic. This is the result of additional $p_x - p_y\pi/\pi^*$ states of sp-hybridized carbons in GD, which allows them to strongly bind the TM adatom and easily trap in within the alkyne rings.

The minimum distances between Fe and the nearest-neighbor carbon atom are listed in Table 2. The height (h) of adatom from the plane of carbon atoms in both cases is obviously smaller than the value of ∼1.48 Å for TM–graphene [21] and TM–CNT [22]. As a result, Fe makes stronger bonds with pGD/GDNT. According to the results of Table 2, the adsorption energy of Fe atom on pGD/GDNT, calculated by DFT + U method (E^U_{ads}), is considerably different from DFT method ($U = 0$). On the other hand, both DFT and DFT + U methods predict that Fe atom has larger adsorption energy with GDNT than with pGD. This is a curvature effect, which causes stronger interactions between p_z orbitals of carbon and 3d orbitals of Fe.

3.2 Electronic properties

The spin-polarized band structures calculated for GDNT and pGD are shown in Fig. 3. The minimum gap between the lowest conduction band and the highest valance band occurs at the Γ point for pGD (0.53 eV) and at the Γ and Z points for GDNT (0.012 eV). For pGD, the highest valance band and the lowest conduction band are both doubly degenerated and consist mainly of $2p_z$ atomic orbitals. For GDNT, on the other hand, the valence and

conduction bands are not degenerated. Similar properties have been observed for graphyne nanotubes [15, 23]. Both systems are non-magnetic, i.e., their spin-up and spin-down bands coincide.

The electron transfer between Fe adatom and pGD/GDNT strongly affects magnetic properties of TM-adsorbed systems. As mentioned above, both pGD and GDNT systems have zero magnetic moments, but the magnetic moment is nonzero when Fe adsorbs (Table 3). In agreement with the results of TM adsorption on graphyne and graphdiyne surfaces [24], the magnetic moments are mainly contributed by Fe atoms. Spin-resolved band structures for Fe-adsorbed pGD and GDNT are shown in Fig. 4. They show semimetallic behavior. Majority spin channels of both systems are metals, but there is a small gap in their minority-spin band structures (Table 3).

Since the 3*d* orbitals of Fe are strongly localized, Hubbard (+U) correction for the correlation energy was employed to account for the effect of the on-site Coulomb repulsion for Fe 3*d* orbitals. As documented in previous works [25–27], compared with the standard DFT method, DFT + U provides a better representation of the ground-state properties of correlated systems. The results of the DFT + U method sensitively depend on the numerical value of the effective on-site electronic interaction, U_{eff} [28]. In this work, the linear response approach [29] was used for the calculation of U_{eff}. For this purpose, localized perturbations (α) were applied and the interacting (χ) and non-interacting (χ_0) density response functions were calculated from the following relation:

$$\chi = \partial n / \partial \alpha \tag{1}$$

where n is the charge density (d occupation). Then, the parameter U_{eff} can be obtained from the formula $U_{\text{eff}} = \chi^{-1} - \chi_0^{-1}$. The calculated values of U_{eff} for pGD and GDNT are 5.23 and 3.68 eV, respectively.

The results of DFT + U calculations are presented in Table 3. The results in Table 3, together with the band structures in Fig. 4, indicate that all the magnetic and electronic properties are very sensitive to the value of U. The band gap (E_g) is obviously increased by considering the U_{eff} parameter. The opening of the band gap due to on-site Coulomb repulsion has been reported before [30]. Moreover, the charge transferred from Fe to pGD/GDNT and the net magnetic moments of the system are larger with the DFT + U method. In this case, a finite correlation of delocalization of electrons in d orbitals of Fe atom causes more splitting in spin-degenerate energy levels, and this

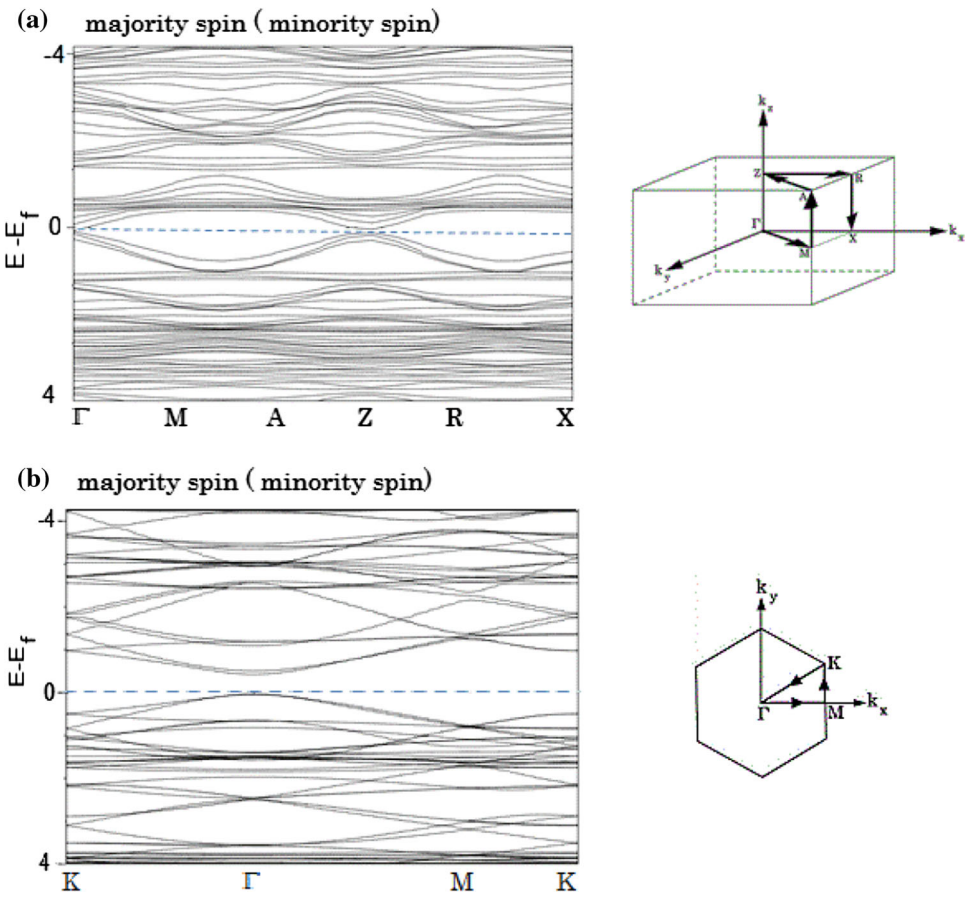

Fig. 3 Band structures of GDNT (**a**) and pGD (**b**). The corresponding Brillouin zones and high symmetry points are illustrated at the *left side* of band structures

Table 3 Amount of charge transferred from Fe to pGD/GDNT (T_e), the band gap (E_g), the net magnetic moment (μ_B) and the Fe atom's valence electron configuration from Löwdin charge analysis for Fe-pGD/GDNT systems

Property	Fe@pGD	Fe@GDNT
T_e (e)	0.821 (1.033)	0.923 (1.915)
E_g (eV)	0.011 (1.098)	0.250 (0.981)
μ_B	2.80 (3.01)	2.01 (2.69)
4*s*3*d*4*p* populations	2.33/6.86/6.39 (2.33/6.53/6.39)	2.36/6.35/6.86 (2.36/6.29/6.86)

The values obtained from the DFT + U method are given in parentheses

splitting of the spin-excitation energy results larger magnetic moment. According to the Löwdin charge analysis of the system, the occupations of 3*d* atomic orbital for Fe atom are reduced with DFT + U calculations, indicating lower electron injection from Fe to pGD/GDNT. These results confirm the stability of Fe-adsorbed systems, which is sensitive to the changes in the *U* parameter.

To understand the origin of magnetism in Fe-pGD/GDNT, projected densities of states (PDOS) for Fe atom and its nearest-neighbor carbon atoms, shown in Fig. 5, can be used. For the majority spin, the *d* orbitals of Fe are strongly coupled with the in-plane p_x and p_y and out of plane p_z orbitals of its nearest-neighbor atoms. However, for the minority spin, there is a large overlap between *d* orbitals.

3.3 Charge transport behavior

The band structures shown in Fig. 3 for pGD and GDNT indicate that they are direct band-gap semiconductors. It is notable that the band gap of semiconductors is underestimated by the density functional theory calculations due to neglecting the self-energy term from many-electron interactions. Despite this deficiency, many theories and computational schemes have been applied successfully for the prediction of intrinsic carrier mobilities of nanostructures [31–35] and yielded values in reasonable agreement with the experimentally measured values [36]. In fact, the dependency of DP constant on relocation of inner energy bands and approximate independency of DP constant of magnitude of band gap provides the possibility of

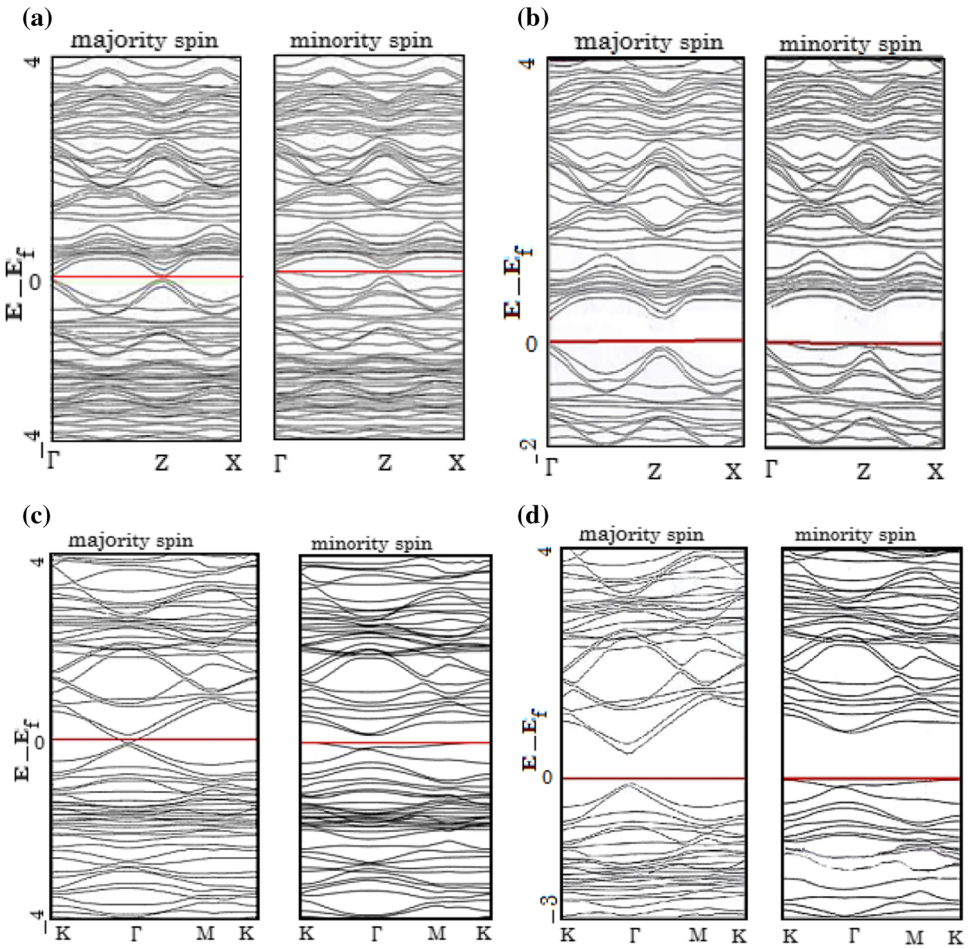

Fig. 4 Spin-polarized band structures of **a** Fe@GDNT from DFT method, **b** Fe@GDNT from DFT + U method, **c** Fe@pGD from DFT method and **d** Fe@pGD from DFT + U method. *Red lines* represent the position of the Fermi level

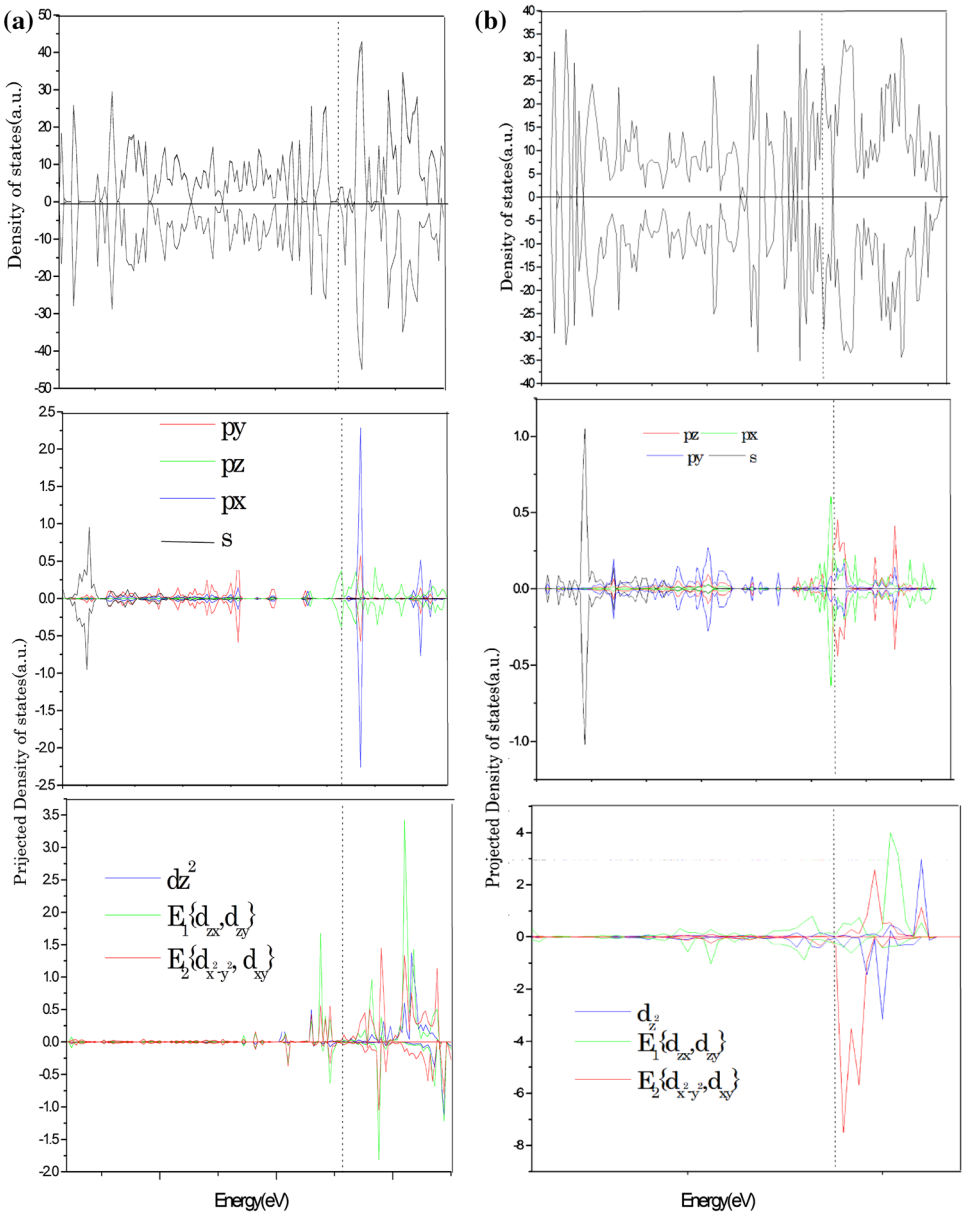

Fig. 5 Spin-polarized density of states for Fe@pGD (**a**) and Fe@GDNT (**b**). From the top to the bottom, the *plots* represent total density of states, projected density of states for carbon atoms near Fe and projected density of states for Fe atom. *Upper* and *lower panels* are for spin-up and spin-down states, respectively, and the Fermi level is at zero energy

calculating transport properties in that situation which band-gap value is calculated by even an error [10, 37]. Boltzmann transport equation (BTE) is among these theories, as a density-functional-based approach has been used for predicting the carrier mobilities in single-walled carbon nanotubes [38] and MoS_2 nanotubes [39].

In the BTE method, the carrier mobility μ in the relaxation time approximation can be written as [40, 41]:

$$\mu_{\alpha}^{e(h)} = \frac{e}{k_B T} \frac{\sum_{i\in CB(VB)} \int \tau_{\alpha}(i,\mathbf{k}) v_{\alpha}^2(i,\mathbf{k}) \exp[\mp\varepsilon_i(\mathbf{k})/k_B T] d\mathbf{k}}{\sum_{i\in CB(VB)} \int \exp[\mp\varepsilon_i(\mathbf{k})/k_B T] d\mathbf{k}} \quad (2)$$

where α is the direction of external field, and $\varepsilon_i(\mathbf{k})$ and $v_{\alpha}(i, \mathbf{k})$ are band energy and the α component of group velocity at state $\mathbf{k}$ of the band i, respectively. The minus (plus) sign is for electron (hole) and the summations run over conduction band (CB) for electrons and valence band (VB) for holes. The integration of $\mathbf{k}$ states is over the first Brillouin zone (BZ). $\tau_{\alpha}(i, \mathbf{k})$ is the relaxation time, which is obtained from the following relation [10]:

$$\frac{1}{\tau_{\alpha}(i,\mathbf{k})} = k_B T \frac{2\pi E_d^2}{\hbar C^{\beta}} \sum_{\mathbf{k}'\in BZ} \left\{ \left[1 - \frac{v_{\alpha}(\mathbf{k}')}{v_{\alpha}(\mathbf{k})} \right] \delta[\varepsilon(\mathbf{k}') - \varepsilon(\mathbf{k})] \right\} \quad (3)$$

In this equation, E_d is the deformation potential (DP constant) for the ith band and C^{β} is the elastic constant along the direction β.

To obtain accurate carrier mobilities, the energy grids on a very fine $\mathbf{k}$-mesh are needed. We chose to calculate the electronic states $\varepsilon_i(\mathbf{k})$ from non-self-consistent calculations

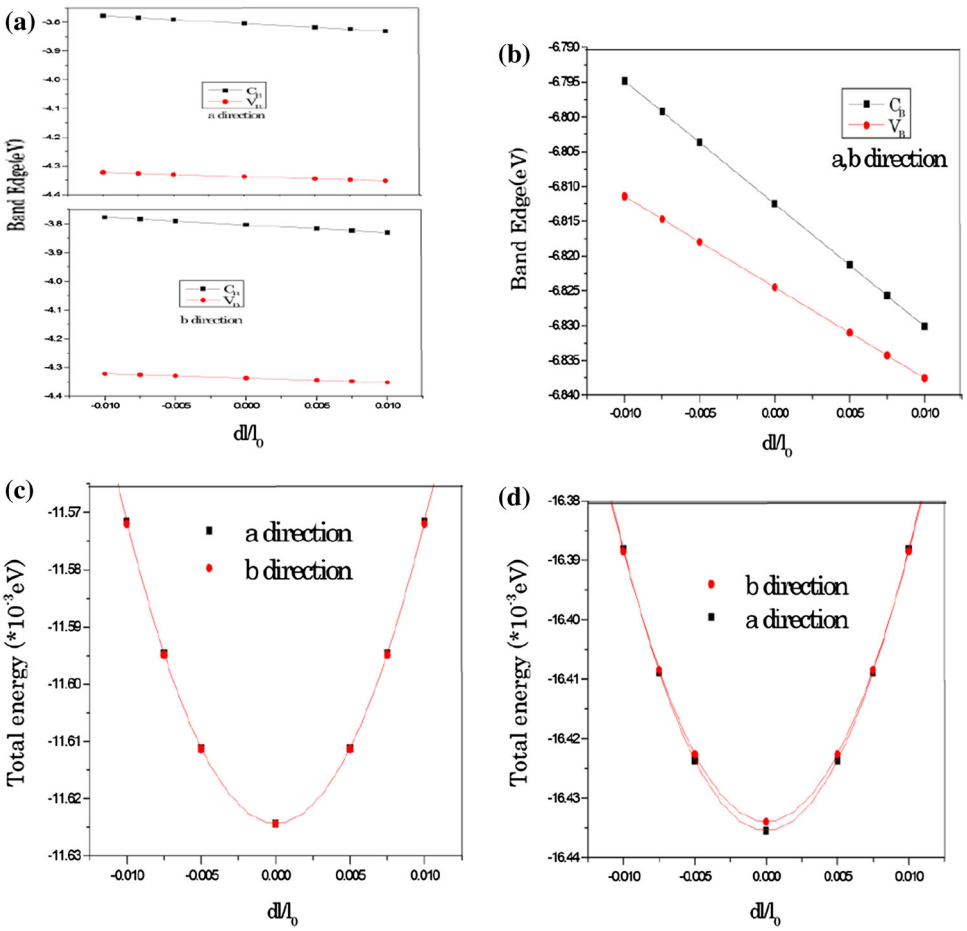

Fig. 6 Band edge position of VB and CB with respect to the lattice dilation along two directions for pGD (**a**) and GDNT (**b**). The linear fit of the data gives the DP constant for electron in VB and for hole in CB. The total energy of a unit cell as a function of lattice deformation along two directions is given in *lower panels* for pGD (**c**) and GDNT (**d**). The quadratic fit of the data gives the elastic constant

on a 81 × 81 × 1 grid for pGD and a 1 × 1 × 111 grid for GDNT. The group velocity of electron and hole carriers can be obtained from $v(i, \mathbf{k}) = \nabla\varepsilon_i(\mathbf{k})/\hbar$ [10]. To calculate the DP constant E_d and the stretching modulus C^β, the supercell was uniformly dilated along the directions **a** and **b** (see Fig. 2) and band structure calculation was performed at different degrees of dilation. The elastic constant of the system along the transport direction β can be obtained by fitting the curve of the total energy E of the supercell with respect to dilation $\Delta l/l_0$, using the following equation:

$$A_0 C^\beta = 2(E - E_0)/(\Delta l/l_0)^2 \quad (4)$$

A_0 and E_0 are area and total energy of the supercell at the optimized structure, respectively. Δl is the deformation of the lattice constant along the direction β, and l_0 is its value at equilibrium geometry. The DP constant is evaluated from $E_d = \Delta E/(\Delta l/l_0)$, where ΔE is energy shift of the band edge position along the direction β.

Figure 6 shows the plots used for the calculation of elastic and DP constants, and the obtained values are given in Table 4. According to the data, elastic constants along two directions are typically very close together for pGD. On the other hand, for GDNT, the elastic constant along **a** direction is lower. Fe adsorption increases the elastic constant for pGD and the **b** direction of GDNT. The DP constant (E_d) characterizes the coupling strength of the charge carriers with the acoustic phonons. The DP constants of pGD and GDNT for electrons and holes are different because these structures are semiconductors. The DP constants along two directions are equal for all systems (Table 4).

Table 4 also shows the relaxation times and carrier mobilities for different systems. For pGD, the charge carriers are delocalized and when the carriers are accelerated by a perturbation, they are subject to scattering by phonons. The DP constants of both pGD and GDNT are larger than the corresponding values for graphene and carbon nanotube [41, 42]. This can be attributed to the fact that the *sp* triple bonds are stronger than the sp^2 double bonds. The elastic and DP constants together can determine the electron–phonon coupling strength [43]. According to Table 4, smaller elastic constant and a much smaller DP constant for GDNT lead to weaker electron–phonon coupling in GDNT than in pGD. This feature may encourage the researchers to further study TM-GDNT systems in order to reach an even smaller E_d (and also higher carrier mobility). In addition,

Table 4 Calculated elastic constants (C^{β}), carrier mobilities (μ), relaxation times (τ) and DP constants (E_d) for electron (e) and hole (h) carriers at 300 K

	pGD	Fe@pGD	GDNT	Fe@GDNT
C^{β} (10^{10} eV cm^{-2})	1.56 (1.57)	1.70 (1.71)	1.39 (1.93)	1.19 (2.04)
μ_h^{β} (10^4 cm^2 V^{-1} s^{-1})	1.163 (1.197)	1.195 (1.204)	0.044 (0.075)	0.966 (0.991)
μ_e^{β} (10^4 cm^2 V^{-1} s^{-1})	21.420 (19.311)	23.331 (21.229)	35.041 (35.003)	37.325 (37.299)
τ_h^{β} (ps)	2.038 (1.987)	2.192 (2.011)	2.057 (1.994)	2.094 (1.863)
τ_e^{β} (ps)	19.936 (15.470)	20.044 (17.095)	20.871 (19.948)	20.997 (19.998)
$E_{d,h}$ (eV)	6.31	8.21	5.21	6.91
$E_{d,e}$ (eV)	2.06	3.95	2.09	1.87

β is an index that denotes **a** and **b** directions, and the values in parentheses are for **b** direction

for all cases, the carrier coupling with acoustic phonons is higher for holes than for electrons.

According to Eq. (2), the intrinsic carrier mobilities depend not only to the relaxation times, but also to the group velocities and the shapes of the Fermi surface. The results show that the carrier mobility of the GDNT in **a** direction is higher than that of pGD for both electrons and holes. The carrier mobility along **a** direction is higher than the mobility along **b** direction in pGD. However, in GDNT, the mobilities along both directions have nearly equal values. Upon the adsorption of Fe, the carrier mobilities increase significantly. So transport in the Fe-adsorbed GDNT is more favorable than in pure GDNT.

4 Conclusions

In conclusion, the electronic and structural properties of a graphdiyne nanotube and a single-layer graphdiyne sheet have been studied. Adsorption of TM can effectively modulate the structural and electrical properties of these structures. High stability in all cases is originated from carbon–carbon triple bonds. We have calculated the intrinsic charge carrier mobility of transition metal-adsorbed graphdiyne in tubular and planar forms scattered by the longitudinal acoustic phonons, using density functional theory and the Boltzmann transport equation with the relaxation time approximation. Our numerical results indicate that charge carrier mobility of zigzag (3, 3) GDNT is larger than pGD. Also, our theoretical results suggest that GDNT exhibits carrier mobility larger than that of a carbon nanotube.

Acknowledgments This research was enabled in part by support provided by *WestGrid* (www.westgrid.ca) and *Compute Canada Calcul Canada* (www.computecanada.ca).

References

1. R.H. Baughman, H. Eckhardt, M. Kertesz, J. Chem. Phys. **87**, 6687 (1987)
2. M. Iyoda, J. Yamakawa, M.J. Rahman, Angew. Chem. Int. Ed. **50**, 10522 (2011)
3. X. Qian, Z. Ning, Y. Li, H. Liu, C. Ouyang, Q. Chen, Y. Li, Dalton Trans. **41**, 730 (2012)
4. S.W. Cranford, M.J. Buehler, Nanoscale **4**, 4587 (2012)
5. M.M. Haley, J.J. Pak, S.C. Brand, Top. Curr. Chem. **201**, 81 (1999)
6. Z.-G. Shao, X.-S. Ye, L. Yang, C.-L. Wang, J. Appl. Phys. **114**, 093712 (2013)
7. H. Du, Z. Deng, Z. Lü, Y. Yin, L. Yu, H. Wu, Z. Chen, Y. Zou, Y. Wang, H. Liu, Y. Li, Synth. Met. **161**, 2055 (2011)
8. A.L. Ivanovskii, Prog. Solid State Chem. **41**, 1 (2013)
9. G. Li, Y. Li, X. Qian, H. Liu, H. Lin, N. Chen, Y. Li, J. Phys. Chem. C **115**, 2611 (2011)
10. M. Long, L. Tang, D. Wang, Y. Li, Z. Shuai, ACS Nano **5**, 2593 (2012)
11. J. He, P. Zhou, N. Jiao, S.Y. Ma, K.W. Zhang, R.Z. Wang, L.Z. Sun, Sci. Rep. **4**, 4014 (2014)
12. D. Vanderbilt, Phys. Rev. B **41**, 7892 (1990)
13. P. Giannozzi, S. Baroni, N. Bonini, M. Calandra, R. Car, C. Cavazzoni, D. Ceresoli, G.L. Chiarotti, M. Cococcioni, I. Dabo, A. Dal Corso, S. de Gironcoli, S. Fabris, G. Fratesi, R. Gebauer, U. Gerstmann, C. Gougoussis, A. Kokalj, M. Lazzeri, L. Martin-Samos, N. Marzari, F. Mauri, R. Mazzarello, S. Paolini, A. Pasquarello, L. Paulatto, C. Sbraccia, S. Scandolo, G. Sclauzero, A.P. Seitsonen, A. Smogunov, P. Umari, R.M. Wentzcovitch, J. Phys. Condens. Matter **21**, 395502 (2009)
14. J.P. Perdew, K. Burke, M. Ernzerhof, Phys. Rev. Lett. **77**, 3865 (1996)
15. V.R. Coluci, D.S. Galvão, R.H. Baughman, J. Chem. Phys. **121**, 3228 (2004)
16. N. Narita, S. Nagai, S. Suzuki, K. Nakao, Phys. Rev. B **58**, 11009 (1998)
17. H.J. Monkhorst, J.D. Pack, Phys. Rev. B **13**, 5188 (1976)
18. MATLAB and Statistics Toolbox Release (2012b) The MathWorks, Inc., Natick
19. R. Saito, G. Dresselhaus, M.S. Dresselhaus, *Physical Properties of Carbon Nanotubes* (Imperial College Press, London, 1998)
20. J. Kunstmann, A. Quandt, I. Boustani, Nanotechnology **18**, 155703 (2007)
21. Y. Mao, J. Yuan, J. Zhong, J. Phys. Condens. Matter **20**, 115209 (2008)
22. H. Valencia, A. Gil, G. Frapper, J. Phys. Chem. C **114**, 14141 (2010)
23. V.R. Coluci, S.F. Braga, S.B. Legoas, D.S. Galvão, R.H. Baughman, Phys. Rev. B **68**, 035430 (2003)
24. J. He, S.Y. Ma, P. Zhou, C.X. Zhang, C. He, L.Z. Sun, J. Phys. Chem. C **116**, 26313 (2012)
25. M.D. Towler, N.L. Allan, N.M. Harrison, V.R. Saunders, W.C. Mackrodt, E. Aprà, Phys. Rev. B **50**, 5041 (1994)
26. O. Bengone, M. Alouani, P. Blöchl, J. Hugel, Phys. Rev. B **62**, 16392 (2000)

27. K. Capelle, V.L. Campo Jr, Phys. Rep. **528**, 91 (2013)
28. S.L. Dudarev, G.A. Botton, S.Y. Savrasov, C.J. Humphreys, A.P. Sutton, Phys. Rev. B **57**, 1505 (1998)
29. M. Cococcioni, S. de Gironcoli, Phys. Rev. B **71**, 035105 (2005)
30. G. Fischer, M. Däne, A. Ernst, P. Bruno, M. Lüders, Z. Szotek, W. Temmerman, W. Hergert, Phys. Rev. B **80**, 014408 (2009)
31. K.I. Bolotin, K.J. Sikes, Z. Jiang, M. Klima, G. Fudenberg, J. Hone, P. Kim, H.L. Stormer, Solid State Commun. **146**, 351 (2008)
32. J.-H. Chen, C. Jang, S. Xiao, M. Ishigami, M.S. Fuhrer, Nat. Nanotechnol. **3**, 206 (2008)
33. M. Orlita, C. Faugeras, P. Plochocka, P. Neugebauer, G. Martinez, D.K. Maude, A.-L. Barra, M. Sprinkle, C. Berger, W.A. de Heer, M. Potemski, Phys. Rev. Lett. **101**, 267601 (2008)
34. Z. Shuai, L. Wang, Q. Li, Adv. Mater. **23**, 1145 (2011)
35. H. Geng, Q. Peng, L. Wang, H. Li, Y. Liao, Z. Ma, Z. Shuai, Adv. Mater. **24**, 3568 (2012)
36. X. Du, I. Skachko, A. Barker, E.Y. Andrei, Nat. Nanotechnol. **3**, 491 (2008)
37. C. Herring, E. Vogt, Phys. Rev. **105**, 1933 (1957)
38. B. Xu, Y.D. Xia, J. Yin, X.G. Wan, K. Jiang, A.D. Li, D. Wu, Z.G. Liu, Appl. Phys. Lett. **96**, 183108 (2010)
39. J. Xiao, M. Long, X. Li, H. Xu, H. Huang, Y. Gao, Sci. Rep. **4**, 4327 (2014)
40. Y.C. Cheng, R.J. Silbey, D.A. da Silva Filho, J.P. Calbert, J. Cornil, J.L. Brédas, J. Chem. Phys. **118**, 3764 (2003)
41. L. Tang, M. Long, D. Wang, Z. Shuai, Sci. China Ser. B **52**, 1646 (2009)
42. L.M. Woods, G.D. Mahan, Phys. Rev. B **61**, 10651 (2000)
43. J. Chen, J. Xi, D. Wang, Z. Shuai, J. Phys. Chem. Lett. **4**, 1443 (2013)